

FULL PAPER

Open Access



# Exploring effects in tippers at island geomagnetic observatories due to realistic depth- and time-varying oceanic electrical conductivity

Rafael Rigaud<sup>1,2\*</sup> , Mikhail Kruglyakov<sup>2,3</sup>, Alexey Kuvshinov<sup>2</sup>, Katia J. Pinheiro<sup>1</sup>, Johannes Petereit<sup>4</sup>, Juergen Matzka<sup>4</sup> and Elena Marshalko<sup>2,5,6</sup>

## Abstract

Vertical magnetic transfer functions (tippers) estimated at island observatories can constrain the one-dimensional (1-D) conductivity distribution of the oceanic lithosphere and upper mantle. This is feasible due to the bathymetry-dependent ocean induction effect (OIE), which originates from lateral conductivity contrasts between ocean and land and leads to non-zero tippers even for 1-D conductivity distributions below the ocean. Proper analysis of island tippers requires accurate three-dimensional (3-D) modeling of the OIE, for which so far was performed assuming constant sea water electric conductivity with depth. In this study, we explore—using rigorous 3-D electromagnetic modeling—to what extent realistic, depth-dependent, oceanic conductivity affects island tippers. The modeling is performed for 11 island observatories around the world in the period range  $10^{-1}$  to  $10^4$  s. We also investigate the effect of seasonal variations of the oceanic conductivity and to which extent this could explain the observed systematic seasonal variation of tippers. Our model studies suggest that for most of the considered island observatories the effect from depth-varying oceanic conductivity is tangible and exceeds the error floor of 0.025, which usually is assigned to tippers during their inversion. The effect varies significantly with location, depending on regional bathymetry. Contrarily, the effects from seasonally varying oceanic conductivity were found to be too small to be worth consideration.

**Keywords:** Ocean induction effect, Tippers, 3-D electromagnetic modeling, Island geomagnetic observatories, Oceanic electrical conductivity

## Introduction

One of the geophysical methods to probe the physical parameters of the Earth's mantle is Geomagnetic Depth Sounding (GDS; Banks 1969; Weidelt 1972). GDS exploits magnetic field variations of magnetospheric and/or ionospheric origin, and allows to constrain electrical conductivity at depth. The main data source for GDS is magnetic field measurements performed at the global net

of geomagnetic observatories. Long-period ( $> 3$  h) variations are routinely used in GDS to constrain electrical conductivity of the Earth's mantle (approximately from 400 km down to 1500 km) either in terms of local one-dimensional (1-D; Olsen 1998; Utada et al. 2003; Munch et al. 2018; Chen et al. 2020; Zhang et al. 2020, among others) or three-dimensional (3-D; Kelbert et al. 2009; Semenov and Kuvshinov 2012; Koyama et al. 2014; Sun et al. 2015; Li et al. 2020, among others) conductivity distributions.

Recent studies (Samrock and Kuvshinov 2013; Morschhauser et al. 2019) have also shown that vertical

\*Correspondence: rafael.rigaud@erdw.ethz.ch

<sup>1</sup> Department of Geophysics, Observatório Nacional, Rio de Janeiro, Brazil  
Full list of author information is available at the end of the article

transfer functions (tippers) estimated from short-period (< 3 h) variations at island observatories can be used to constrain conductivity distribution beneath oceans, where our knowledge is still very limited. This becomes feasible due to the ocean induction effect (OIE; cf. Parkinson and Jones 1979), which originates from lateral conductivity contrasts between ocean and land. The OIE leads to non-zero tippers even for 1-D conductivity distribution beneath the ocean (cf. Samrock and Kuvshinov 2013); therefore, the inversion of island tippers can provide information on the electrical properties of the crust and upper mantle in remote oceanic regions. However, the interpretation of island tippers requires accurate 3-D electromagnetic (EM) modeling of the OIE that takes into account the bathymetry around the observatory. Hitherto, during such modeling, the researchers assumed constant oceanic electric conductivity with depth (cf. Samrock and Kuvshinov 2013; Morschhauser et al. 2019). In many regions of the world, however, oceanic conductivity varies significantly within the uppermost few hundred meters of the water column (cf. Tyler et al. 2017). In this study, we explore the extent to which realistic depth-varying oceanic conductivity affects island tippers. Our analysis is performed for 11 island observatories located in the Pacific, Atlantic, and Indian Oceans (cf. Fig. 1). In addition, we investigate the effect of seasonal variations of oceanic conductivity and to which extent this could explain the systematic seasonal variations in tippers investigated by Araya Vargas and Ritter (2016) and

attributed to the variability of external magnetic source fields.

## Methods

### Tippers

In non-polar regions, the source of the magnetic field variations with periods shorter than 3 h is well approximated by a vertically incident plane wave. The plane-wave assumption allows one to relate the vertical component  $B_z$  with the horizontal component  $\mathbf{B}_H = (B_x, B_y)$  at the location  $\mathbf{r} = (x, y, z)$  via the so-called tipper  $\mathbf{T} = (T_{zx}, T_{zy})$  (e.g., Berdichevsky and Dmitriev 2008):

$$B_z(\omega, \mathbf{r}) = T_{zx}(\omega, \mathbf{r})B_x(\omega, \mathbf{r}) + T_{zy}(\omega, \mathbf{r})B_y(\omega, \mathbf{r}), \quad (1)$$

where  $\omega = 2\pi/P$  is the angular frequency of magnetic field variations with period  $P$ . The  $x$ - and  $y$ -directions are defined in this paper as the directions to geographic North and East, respectively, and  $z$  is directed vertically downwards. As a consequence of the plane-wave excitation,  $B_z$  (and, thus,  $\mathbf{T}$ ) are non-zero only above non-1-D conductivity structures. In fact, one can interpret  $\mathbf{T}$  as a measure of the tipping of the magnetic field out of the horizontal plane above two-dimensional or/and 3-D conductivity structures.

### Global oceanic conductivity model

The global oceanic electric conductivity model used here is that by Petereit et al. (2019), which is based on the Coriolis Oceanographic data set for Re-Analysis

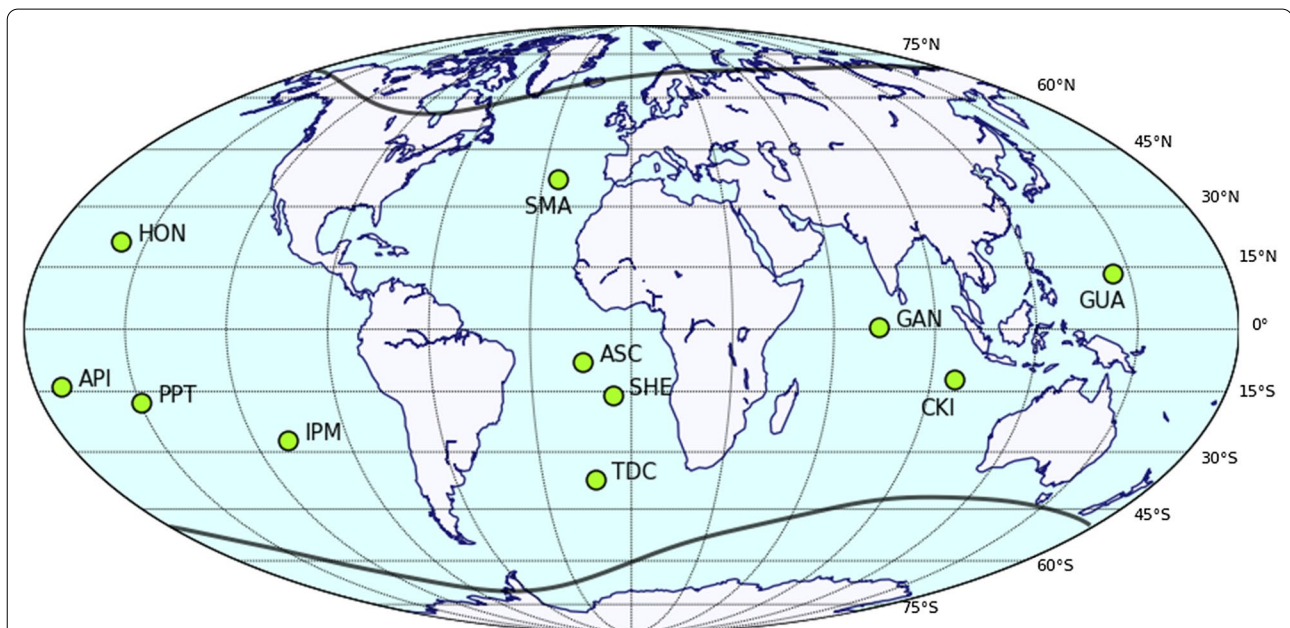


**Fig. 1** Location of geomagnetic observatories used in this study (green dots). Black lines depict  $\pm 55^\circ$  quasi-dipole latitudes. Relevant information about these observatories is summarized in Table 1

(CORA5.0, Cabanes et al. 2013) provided by the Copernicus Marine Environment Monitoring Service. The model consists of monthly 3-D oceanic electrical conductivity distributions from 1990 to 2016. The conductivity is computed on a lateral grid of  $0.5^\circ \times 0.5^\circ$  resolution and at 152 vertical levels between the sea surface and 2000 m. More details on the oceanographic data set and the calculation of the global oceanic conductivity model can be found in Petereit et al. (2019). From 2000 m down to the ocean bottom, the sea water conductivity was set to 3.2 S/m (cf. Tyler et al. 2017). As an example, Fig. 2 presents global maps of the depth-averaged oceanic conductivity for a number of depth intervals for December 2015, illustrating the fact that oceanic conductivity indeed varies laterally and with depth.

### Constructing island 3-D conductivity models

The (Cartesian) 3-D conductivity models were constructed separately for each observatory. The models include a nonuniform oceanic bathymetry and a landmass with a uniform conductivity of 0.01 S/m. We decided to use the same land conductivity for all observatories as a mean representative value, since we did not succeed to find better data to set the land conductivity specific for each location. The landmass is defined here as the upper crust from the maximum elevation down to the maximum depth of the ocean in the considered region. Note that landmass conductivity of 0.01 S/m was also adopted in the previous studies (Morschhauser et al. 2019; Samrock and Kuvshinov 2013) which addressed modeling of island tippers.

The landmass and the ocean comprise the 3-D part of the model, which is underlain by a crust and mantle with the 1-D conductivity distribution (cf. Fig. 3) from Grayver et al. (2017). Their 1-D model was obtained by joint inversion of satellite-detected tidal and magnetospheric signals and is believed to represent the globally averaged 1-D conductivity profile beneath the oceans. More details on our 3-D models are as follows.

First, we note that as far as we exploit the integral equation (IE) based solver (to be discussed in the next section) to compute magnetic fields, the modeling domain is confined to the 3-D part of the model. The lateral size of the 3-D modeling domain was taken as  $356 \times 356 \text{ km}^2$  square with the island observatory in its center. The island was placed in the center of the modeling region (laterally) to avoid potential edge effects in the results. The vertical range of the domain is from the maximum topography down to the maximum depth of the ocean in the region of interest. The 3-D part of the models is constructed using bathymetry and topography data from the General Bathymetry Chart of the Oceans (GEBCO 2019), which is a global map compiled from a variety of sources with 15

arc sec horizontal resolution (corresponding to 0.46 km at the equator). Bathymetry/topography is converted to Cartesian coordinates by the use of the Transverse Mercator map projection and then linearly interpolated to a uniform grid with 1 km horizontal resolution. Note that we performed a comprehensive model study to justify the chosen lateral size of the modeling domain and cell sizes.

The uppermost left panel in Figs. 5, 6, 7, 8, 9, 10, 11, 12, 13, 14 and 15 shows the bathymetry/topography in the vicinity of the corresponding island observatory. Vertically, the 3-D modeling domain was discretized in 100 m layers from the maximum topography down to 1000 m depth; from 1000 m down to the maximum bathymetry in the region, the domain was discretized in 500 m-thick layers (see Fig. 4). Oceanic conductivity within each vertical layer is assumed to be constant and is set to the 3-D average value of the 2015 December (or June) oceanic conductivity model for the layer's volume. The models from 2015 year are chosen, since most of experimental tippers are derived from the data for this year (or adjacent years). Sedimentary layers were not incorporated into the models, since sediment thickness is negligible in the oceanic regions considered in this study (Straume et al. 2019).

Outside the 3-D volume, at depths between the surface and maximum depth of the ocean, conductivity is assumed to be laterally uniform (1-D) and is set to the same oceanic conductivity profile as inside the volume, underlain by the 1-D model for crust and mantle. The air conductivity is set to  $10^{-8}$  S/m. The uppermost right panel in Figs. 5, 6, 7, 8, 9, 10, 11, 12, 13, 14 and 15 depicts the vertical profile of oceanic conductivity (in purple), calculated by horizontally averaging oceanic conductivity (Fig. 2) in a  $5^\circ \times 5^\circ$  region centered at the considered island observatory. The panel demonstrates that the oceanic conductivity varies significantly with depth down to approximately 1 km depth. Below this depth, the values are close to 3.2 S/m.

Furthermore, for each observatory, we construct a 3-D model with a constant oceanic conductivity of 3.2 S/m in all vertical layers. Outside the 3-D volume, the oceanic conductivity is set to 3.2 S/m, underlain by the 1-D model by Grayver et al. (2017) for crust and mantle.

### Modeling tippers

We compute magnetic fields (and then tippers) using the 3-D EM forward modeling solver PGIEM2G which is based on a volume integral equation method with contracting kernel (Pankratov et al. 1995; Singer 1995), and which was presented and validated (against finite-element solver by Grayver and Kolev 2015) in Kruglyakov and Kuvshinov (2018).

We compute tippers at 25 periods spanning the range from  $10^{-1}$  to  $10^4$  s. Note that, nowadays, most observatories provide magnetic field data in the form of minute means. This allows researchers to estimate tippers at periods starting from approximately 300 s. However, there is a growing investment from the scientific community in providing magnetic observatory data in the form of second means, which would enable estimating tippers for periods down to a few seconds. Tippers for even smaller periods can also be estimated at observatory locations by performing a short-term (a few days) measurements with the use of induction coils; note that the standard observatory instrument to measure magnetic field variations is a fluxgate magnetometer. Bearing in mind the above considerations, we modeled tippers at periods shorter than 300 s to obtain an idea what is the smallest period at which ocean induction effect becomes noticeable.

#### Estimating tippers from the data

We estimated tippers at nine island geomagnetic observatories from the International Real-Time Magnetic Observatory Network (INTERMAGNET) using definite minute-mean data that are time-series of three components of magnetic field. In addition, we estimated tippers at two non-INTERMAGNET island observatories: St. Helena (SHE) and Santa-Maria/Azores (SMA), also using minute-mean data. Prior to the tipper estimation, obvious spikes were removed from the corresponding time-series. Table 1 summarizes information about the observatories, including the time interval used for the tipper estimation. This interval varies from observatory to observatory and was selected—based on a trial-and-error approach—to

obtain smooth (with respect to period) tippers with low uncertainties.

For each period, data were split into overlapping tapered windows of two period length. Data in these windows were Fourier transformed, giving the spectrum of the corresponding component from 300 to 9600 s. Tippers and their uncertainties were then estimated using a robust, section-averaging (Olsen 1998) linear regression scheme based on the Huber norm (e.g., Aster et al. 2005; Pütke and Kuvshinov 2014).

## Results

### Effect of depth-varying oceanic conductivity

Modeling results for all 11 island observatories are presented in Figs. 5, 6, 7, 8, 9, 10, 11, 12, 13, 14 and 15. In the figures, panel (a) shows the bathymetry/topography map with the corresponding observatory located in the center. The dashed line indicates the West–East running bathymetry/topography profile, as shown in panel (b). Panel (c) shows the regional depth-varying oceanic conductivity down to 2000 m (purple solid line) and the constant reference oceanic conductivity (3.2 S/m, dashed orange line). Panels (d–g) present the  $\text{Re } T_{zx}$ ,  $\text{Re } T_{zy}$ ,  $\text{Im } T_{zx}$ , and  $\text{Im } T_{zy}$  tipper components. Red and orange curves correspond to tippers calculated in the models with depth-varying and depth-constant oceanic electrical conductivity, respectively. The blue curves represent tippers and their uncertainties estimated from the data. One can see that both observed and modeled tippers fulfill the property (Marcuello et al. 2005) that is often used as a plausibility check for the tippers, namely, at periods where  $\text{Re } T_{zx}$  or  $\text{Re } T_{zy}$  reaches a maximum (or a minimum) value,  $\text{Im } T_{zx}$  or  $\text{Im } T_{zy}$  changes the sign. Finally, panels (h) and (i) show the effect of depth-varying

**Table 1** Information on the geomagnetic observatories used in this study

Code	Name	lat <sup>GG</sup>	lon <sup>GG</sup>	lat <sup>GM</sup>	lon <sup>GM</sup>	Time interval used for tippers' estimation
API	Apia	−13.81	−171.78	−15.05	263.35	01/01/2016 – 31/12/2017
ASC	Ascension Island	−7.95	−14.38	−2.77	57.48	01/01/2014 – 31/12/2015
CKI	Cocos-Keeling Islands	−12.10	96.84	−21.56	168.92	01/01/2017 – 31/12/2018
GAN	Gan	0.69	73.15	−8.64	145.33	01/01/2016 – 31/12/2017
GUA	Guam	13.59	144.87	5.8	216.51	01/01/2017 – 31/12/2018
HON	Honolulu	20.32	−158	21.65	270.85	01/01/2015 – 31/12/2016
IPM	Easter Island	−27.2	−109.42	−19.17	325.61	01/01/2013 – 31/12/2015
PPT	Pamatai	−17.57	−149.58	−15.05	285.79	01/01/2015 – 31/12/2016
SHE	St. Helena*	−15.90	−5.75	11.78	64.24	01/01/2015 – 31/12/2015
SMA	Santa Maria/Azores*	36.99	−25.13	43.21	53.57	01/05/2018 – 31/09/2019
TDC	Tristan da Cunha	−37.07	−12.31	−31.70	54.76	01/01/2013 – 31/12/2014

From left to right: IAGA code, observatory name, geographic and geomagnetic latitude and longitude, and time interval used to estimate tippers. Observatories with an asterisk (\*) are, as of date, not participating in INTERMAGNET and data are available from GFZ Potsdam. Geomagnetic coordinates were calculated using the IGRF-12 model, epoch 2015

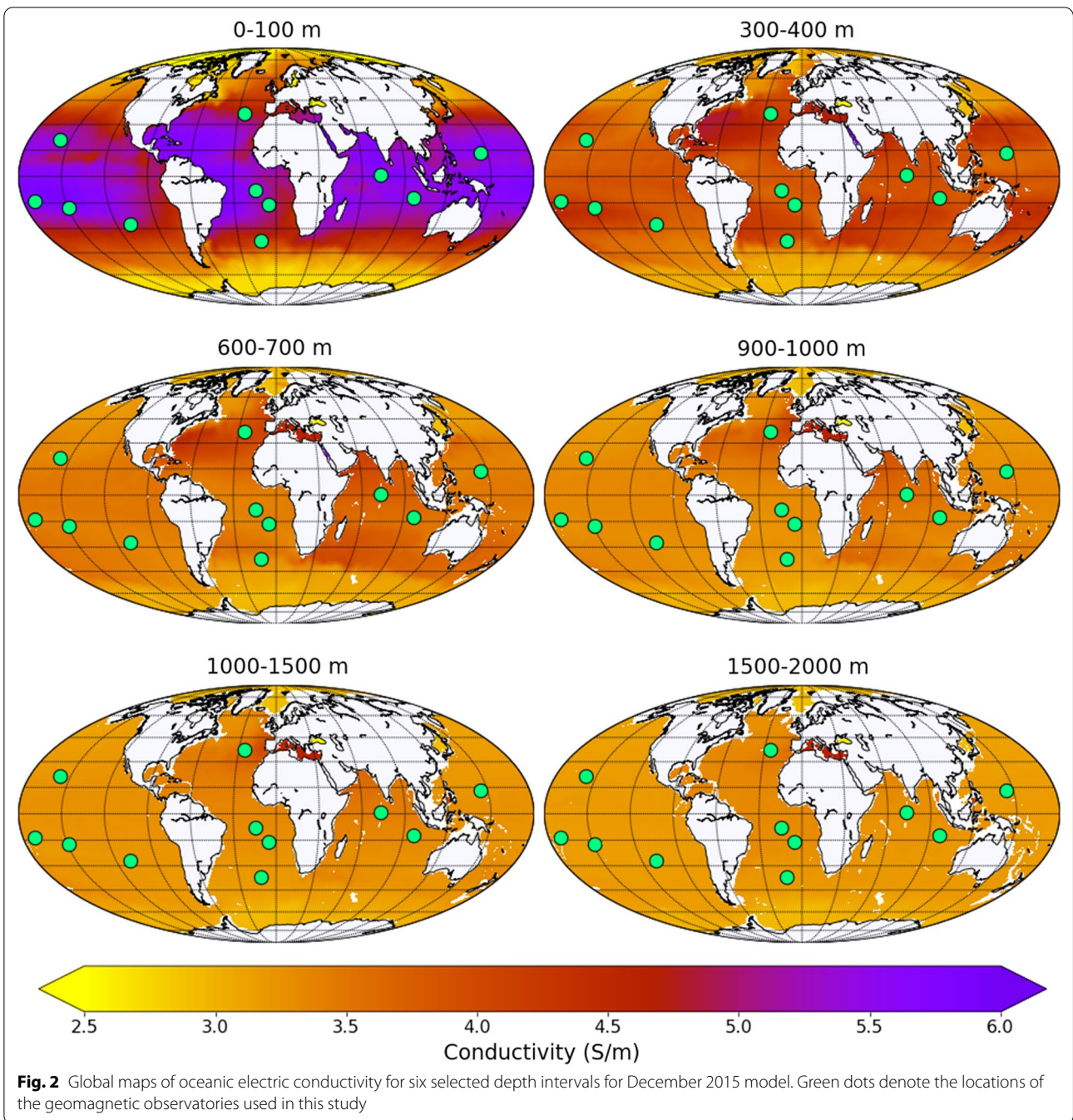


**Fig. 2** Global maps of oceanic electric conductivity for six selected depth intervals for December 2015 model. Green dots denote the locations of the geomagnetic observatories used in this study

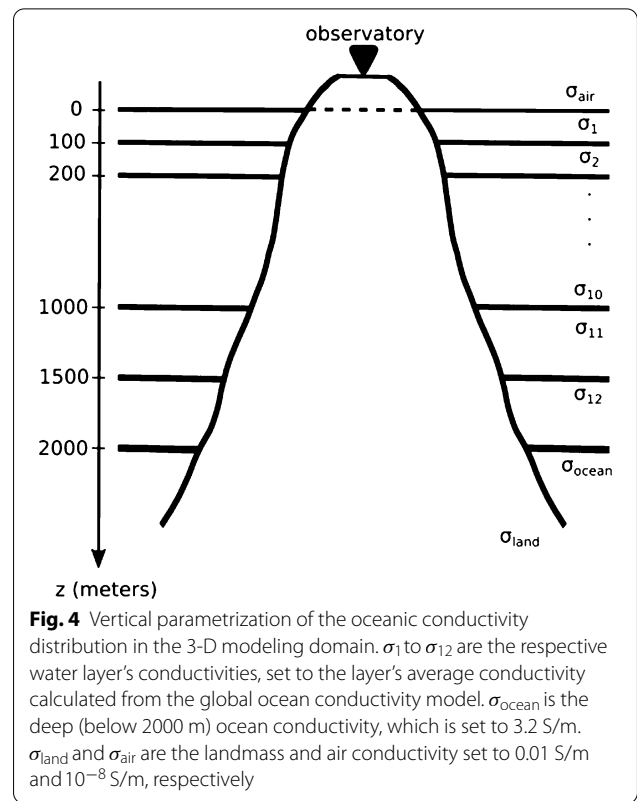
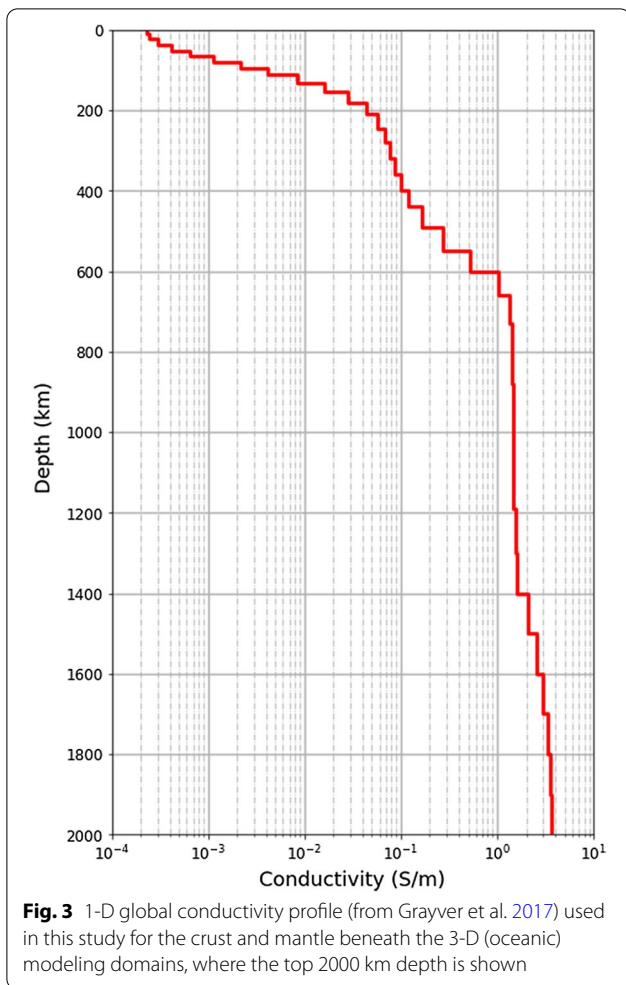
oceanic conductivity on island tippers. This effect is assessed by the following difference:

$$\Delta T_{zi} = \sqrt{(\text{Re } T_{zi}^v - \text{Re } T_{zi}^c)^2 + (\text{Im } T_{zi}^v - \text{Im } T_{zi}^c)^2}, \tag{2}$$

where  $i \in [x, y]$ , and superscripts “v” and “c” correspond to the tippers calculated in the models with depth-varying and depth-constant oceanic conductivity, respectively.

Here, we consider the effect as non negligible if it exceeds a value of 0.025, which is conventionally used as an error floor in tipper inversions (e.g., Morschhauser et al. 2019; Yang et al. 2015; Tietze and Ritter 2013; Rao et al. 2014; Bedrosian and Feucht 2014) and which is shown in the panels as horizontal dashed line.

Three observations can be made from panels (d–g) that are independent of modeling being done with depth-varying or depth-constant oceanic conductivity:



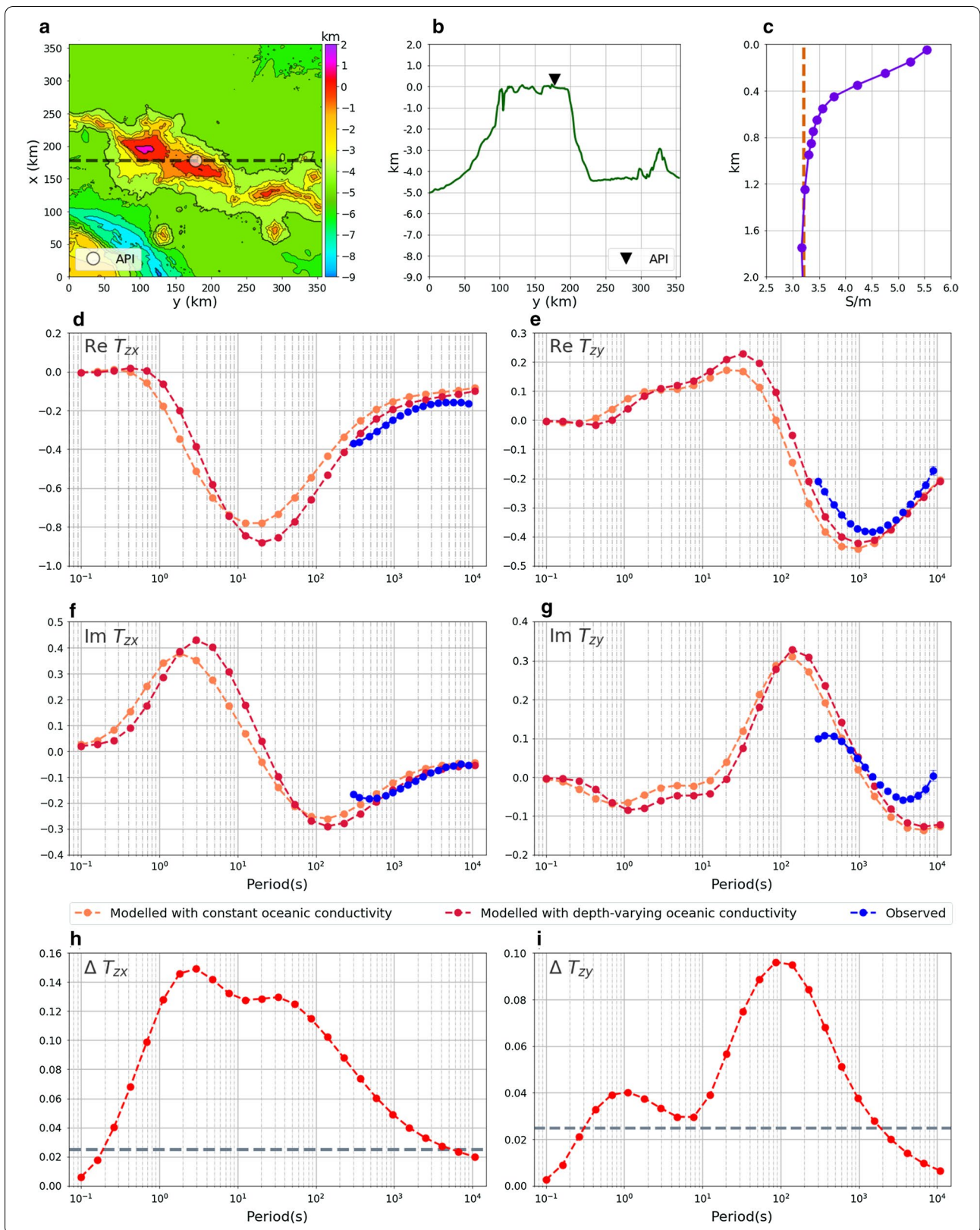
1. The manifestation of the OIE in the modeled tippers varies from observatory to observatory. Given that depth-varying oceanic conductivity profiles (panels (c) in all figures) present similar values for all observatories, except for SMA, this variability of the OIE is expected to be due to the different bathymetry distributions around the islands.
2. Modeled and experimental tippers agree rather well for most observatories, for the full spectrum from 300 to 9600 s, for both components and for both the real and imaginary parts. Any remaining discrepancy

- can most probably be attributed to regional deviations of the crustal and mantle conductivity structure from the global 1-D conductivity structure used for modeling, and, partly, to limitations in bathymetry data resolution.
3. The modeled OIE in tippers can be traced to periods as short as 0.2 s.

As for the effect from depth-varying oceanic conductivity, it varies from observatory to observatory, from component to component, and shows different behaviour with respect to period. This variability, like the variability of OIE itself, is expected to be from the different bathymetry distributions around the islands. The largest effect—reaching 0.15—is observed at Apia observatory in  $Re T_{zx}$  component.

(See figure on next page.)

**Fig. 5** Results for Apia observatory (API). **a** Map of bathymetry/topography; dashed line indicates location of profile shown in **b**. **b** West–East oriented bathymetry profile. **c** Regional depth-varying (purple) oceanic conductivity and constant reference oceanic conductivity (3.2 S/m, orange dashed line). **d–g** Real and imaginary parts for x and y components of tippers computed in the model with depth-varying (red dots and dashed line) and depth-constant (orange dots and dashed line) oceanic conductivity. **h** Difference for the computed tipper x component between depth-varying and depth-constant ocean conductivity, see text for details. Dashed grey line indicates the threshold of 0.025. **i** Same as (**h**), but for the y component



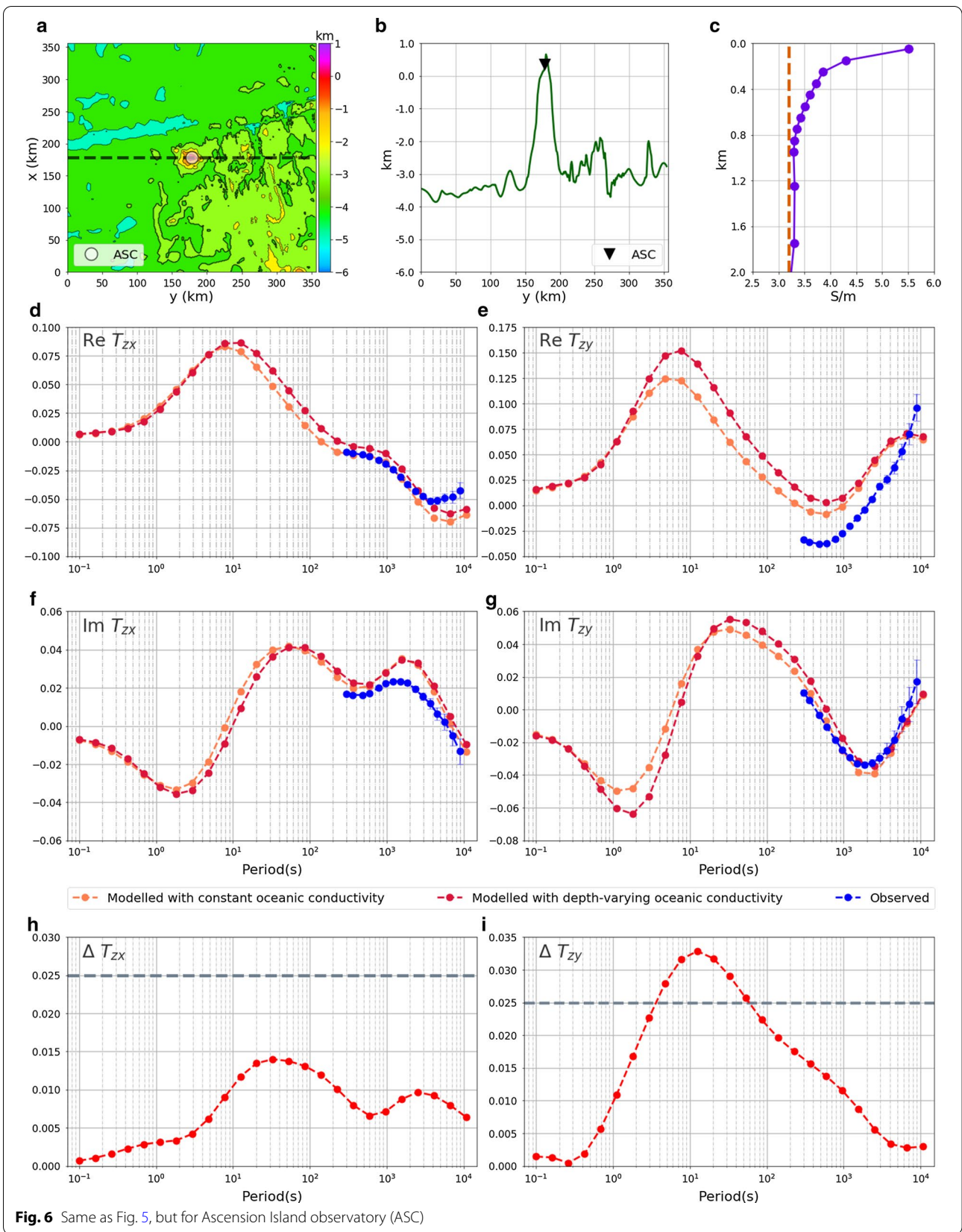


**Fig. 6** Same as Fig. 5, but for Ascension Island observatory (ASC)

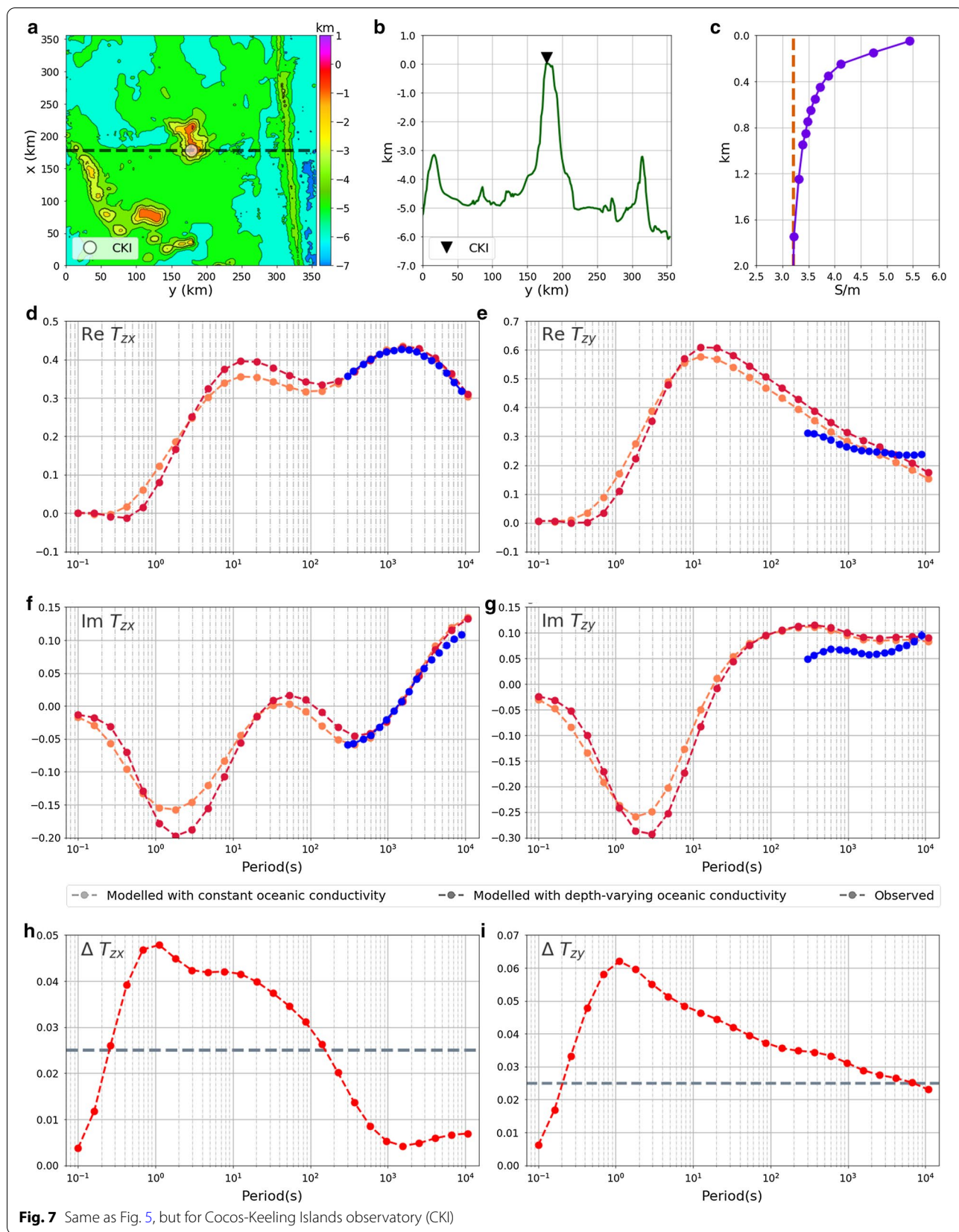


**Fig. 7** Same as Fig. 5, but for Cocos-Keeling Islands observatory (CKI)

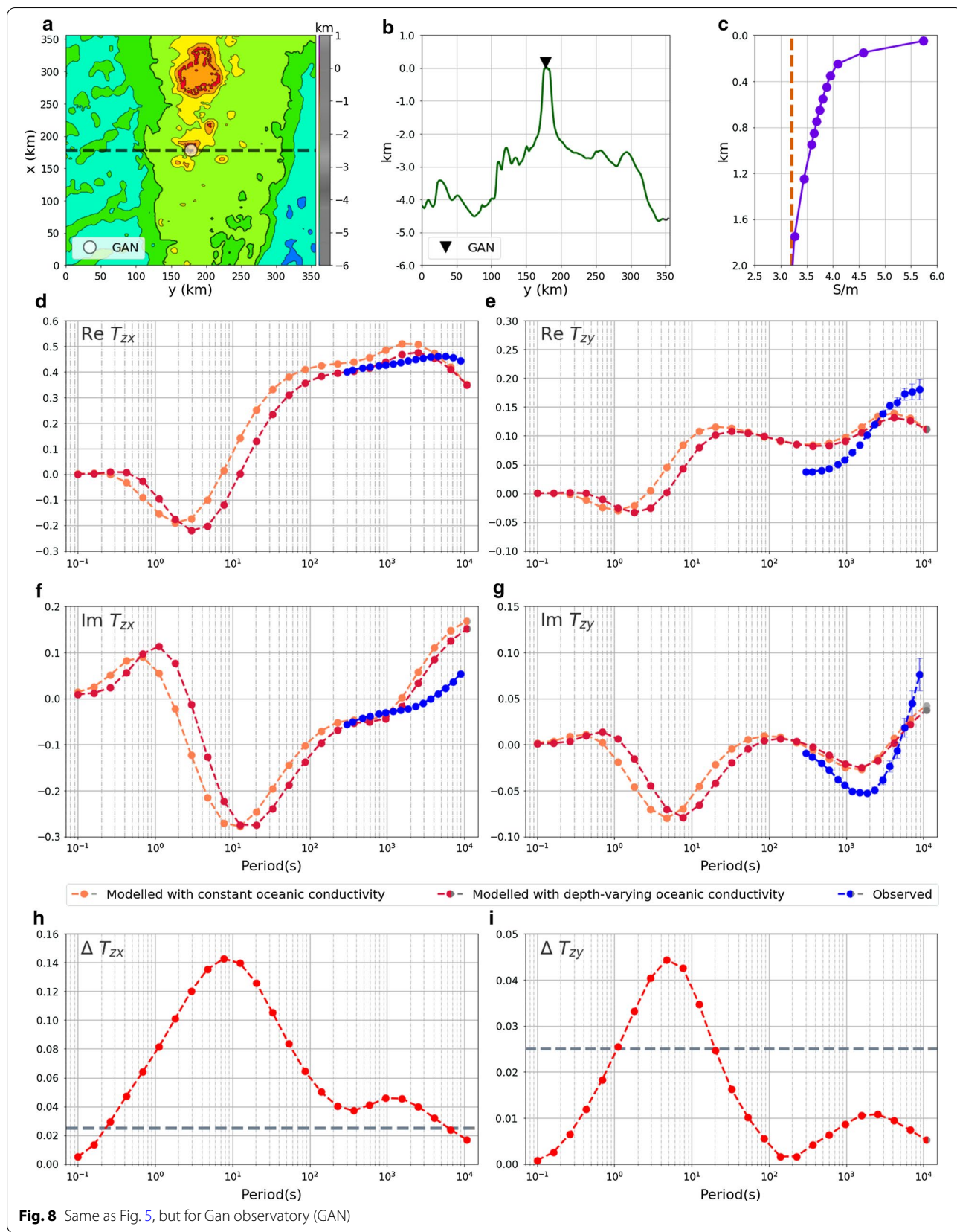


**Fig. 8** Same as Fig. 5, but for Gan observatory (GAN)

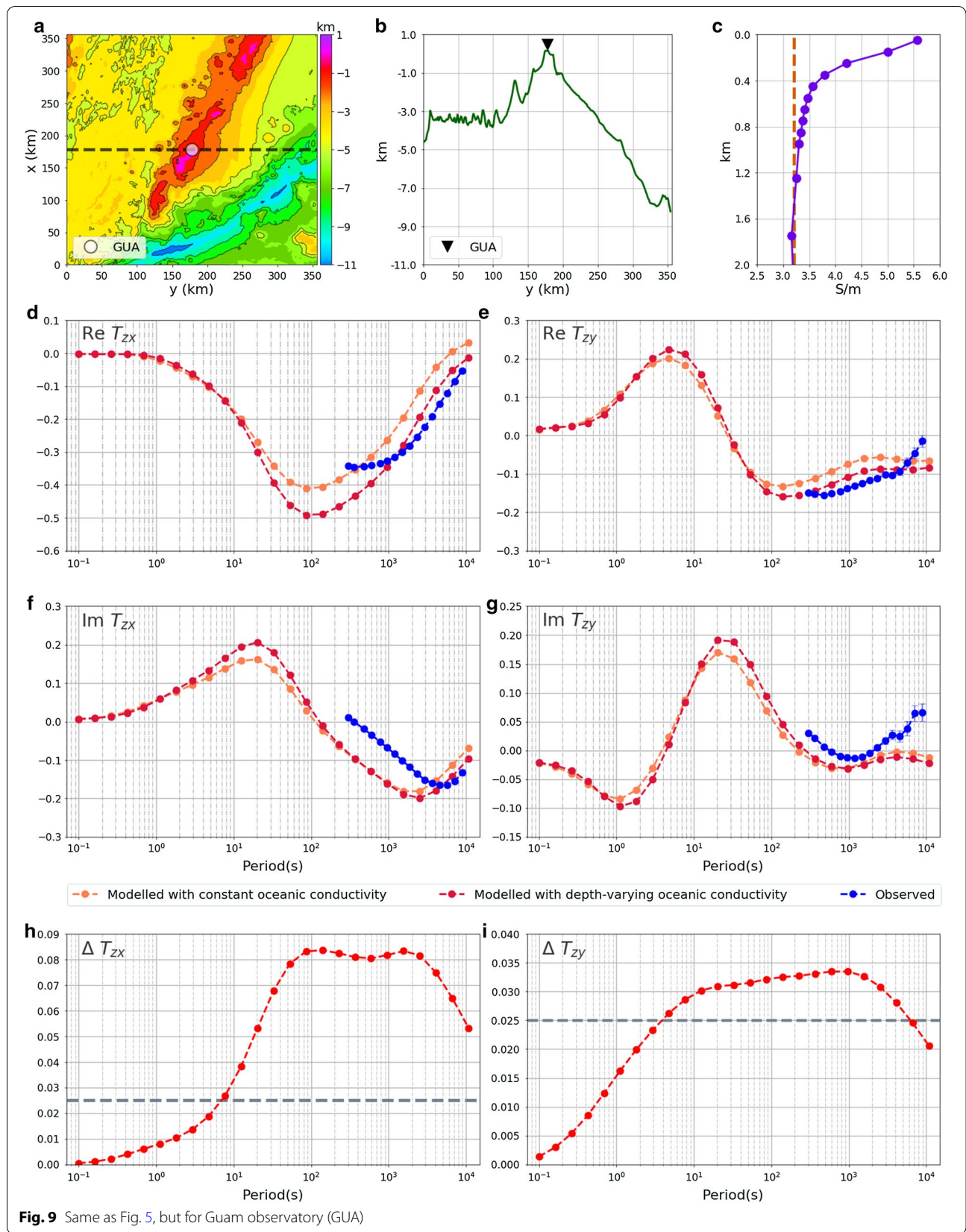


**Fig. 9** Same as Fig. 5, but for Guam observatory (GUA)

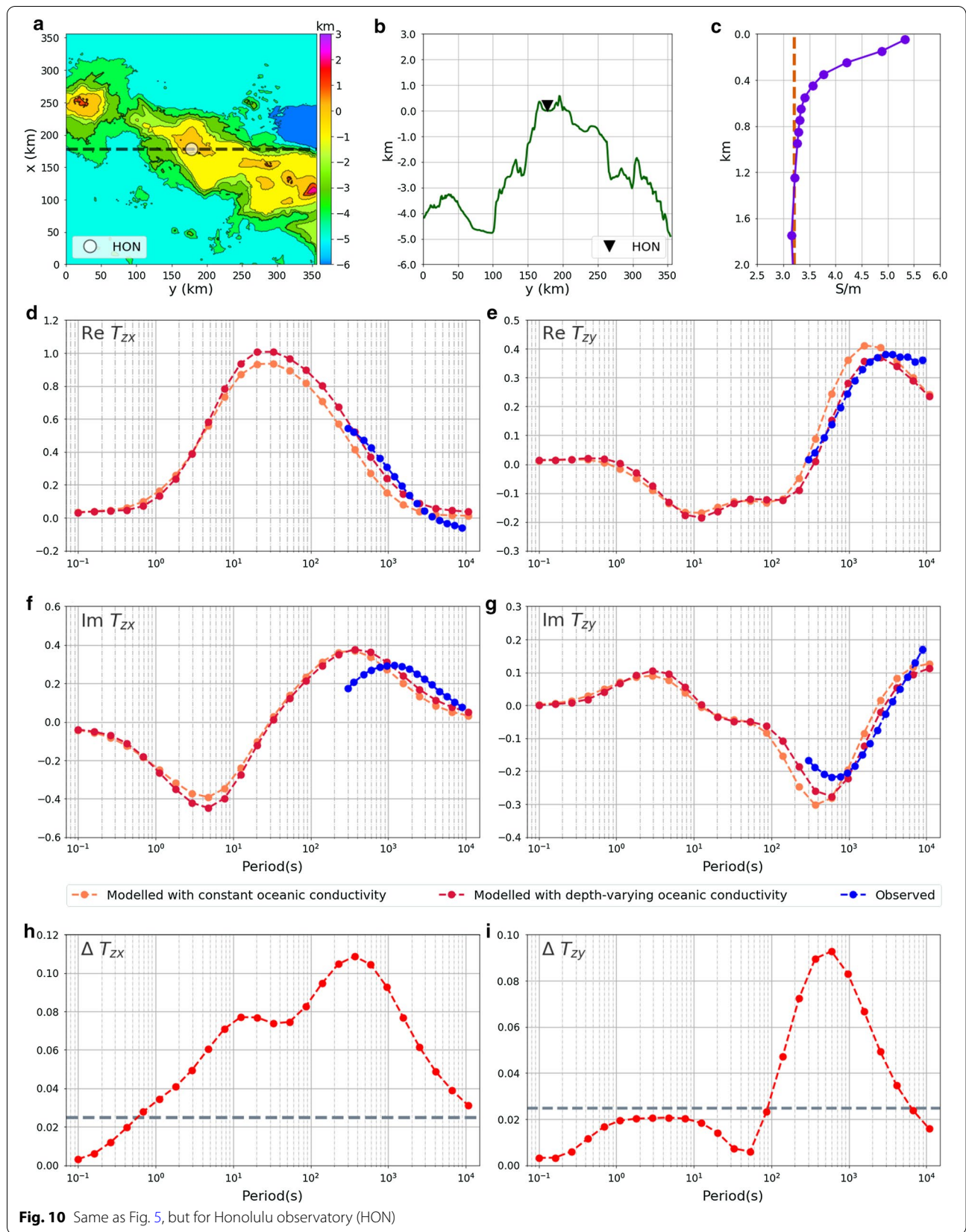


**Fig. 10** Same as Fig. 5, but for Honolulu observatory (HON)

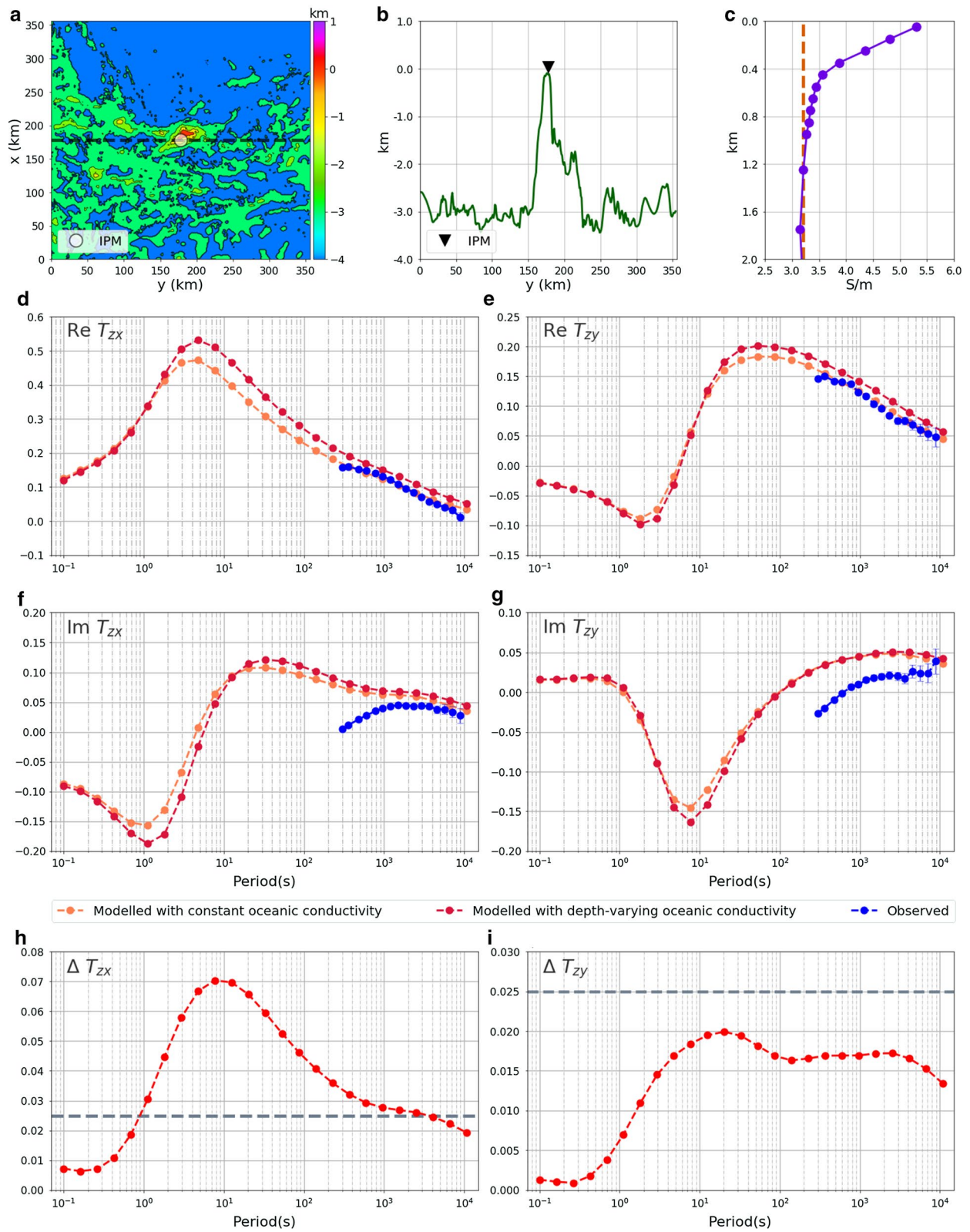


**Fig. 11** Same as Fig. 5, but for Easter Island observatory (IPM)

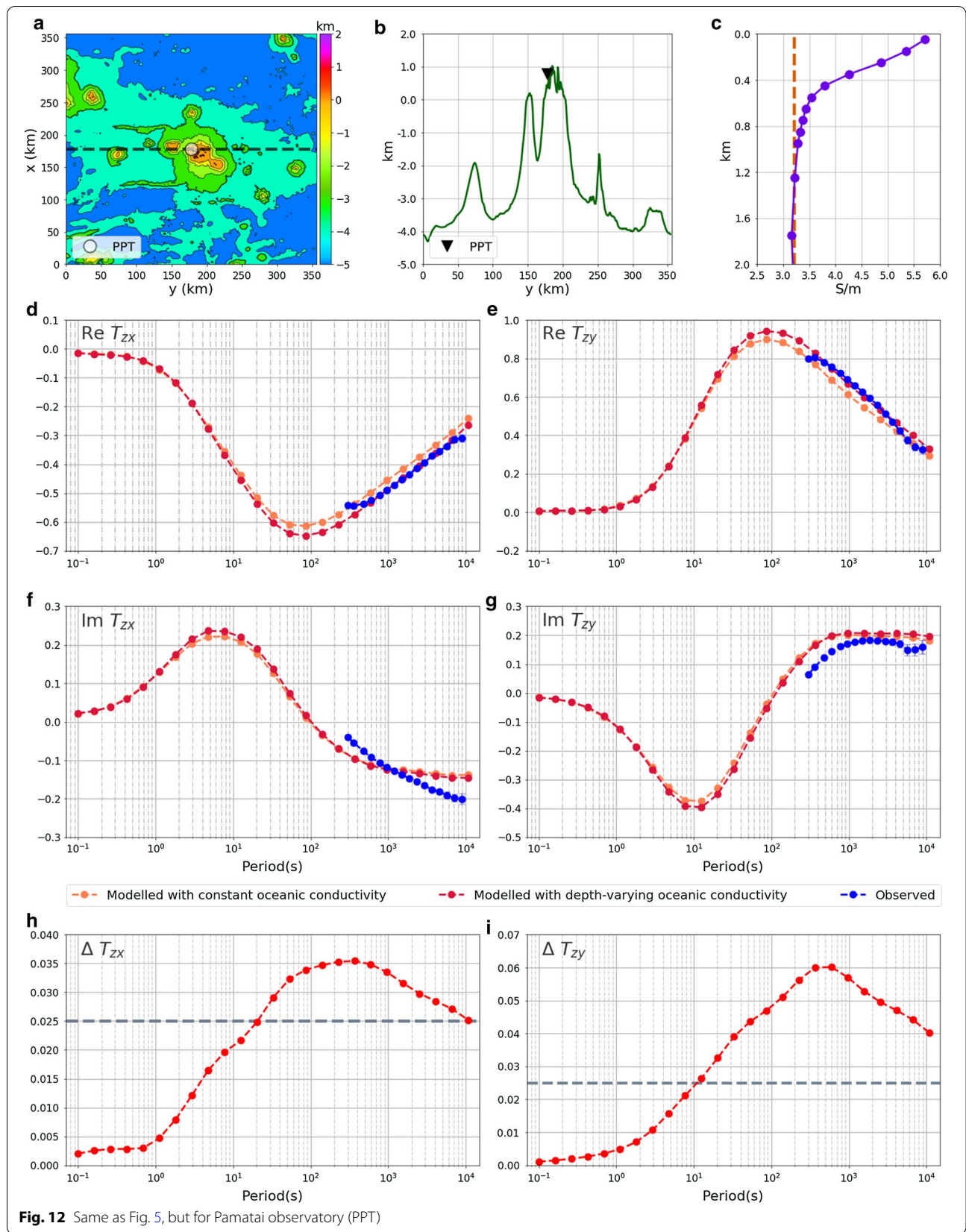


**Fig. 12** Same as Fig. 5, but for Pamatai observatory (PPT)

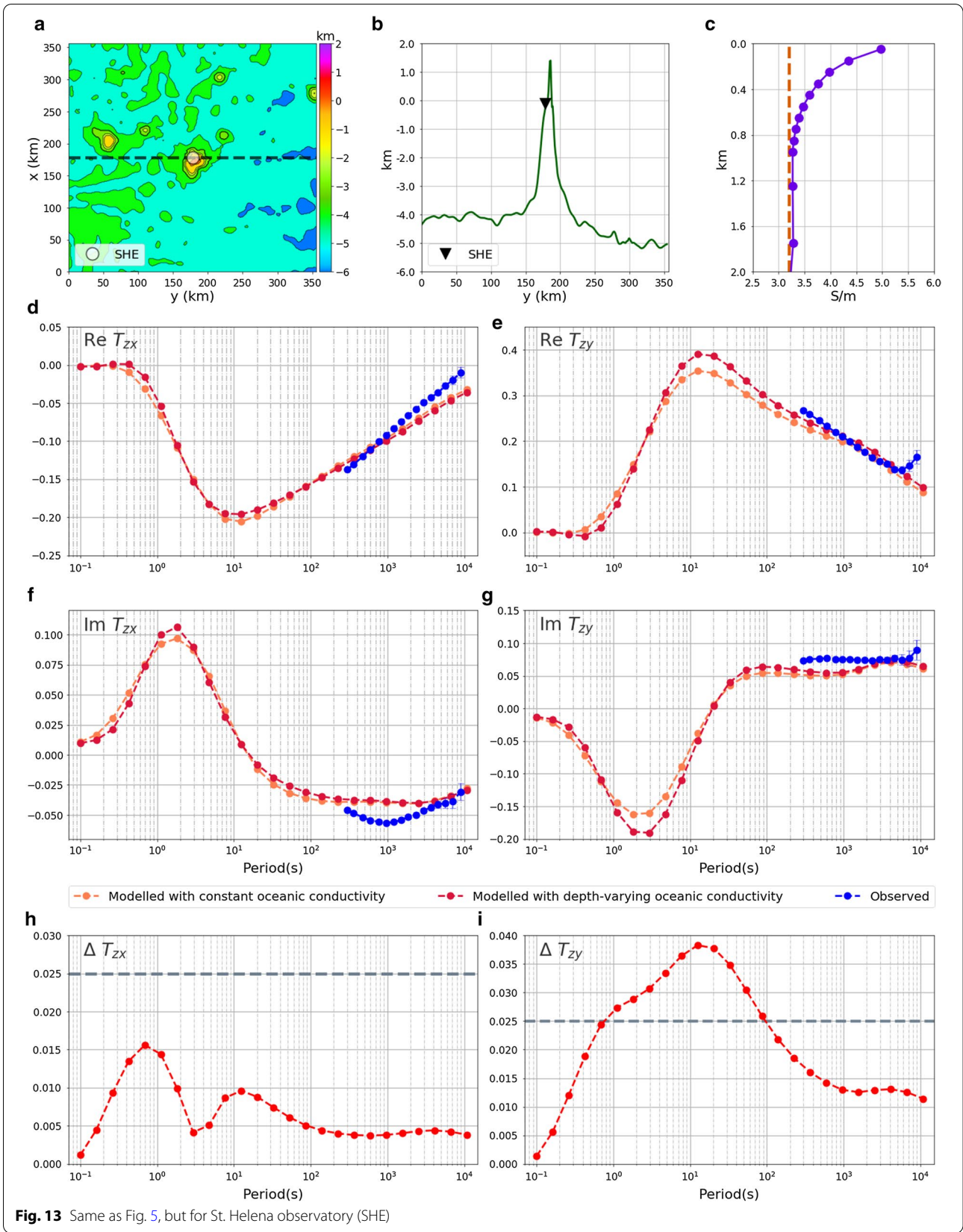


**Fig. 13** Same as Fig. 5, but for St. Helena observatory (SHE)

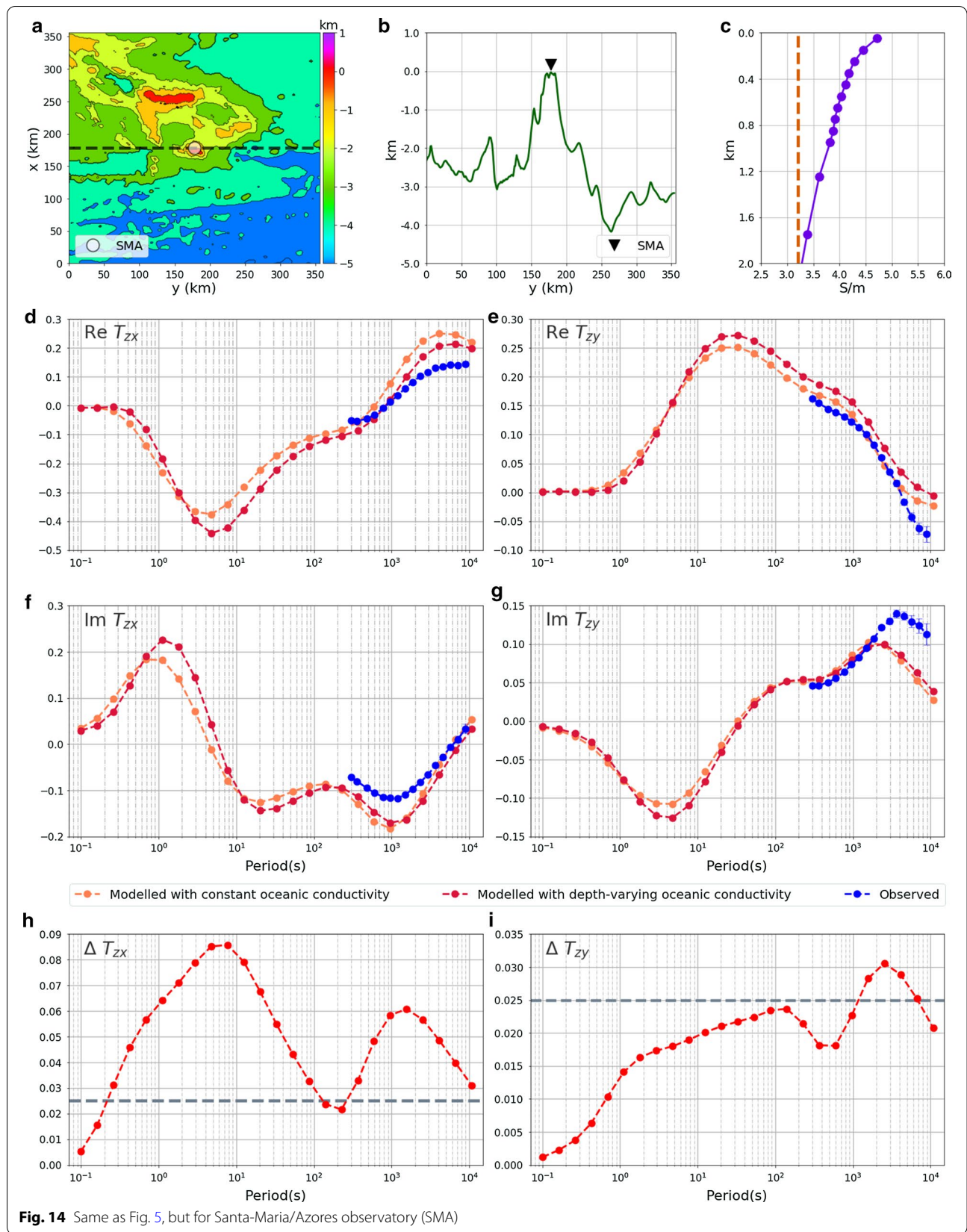


**Fig. 14** Same as Fig. 5, but for Santa-Maria/Azores observatory (SMA)

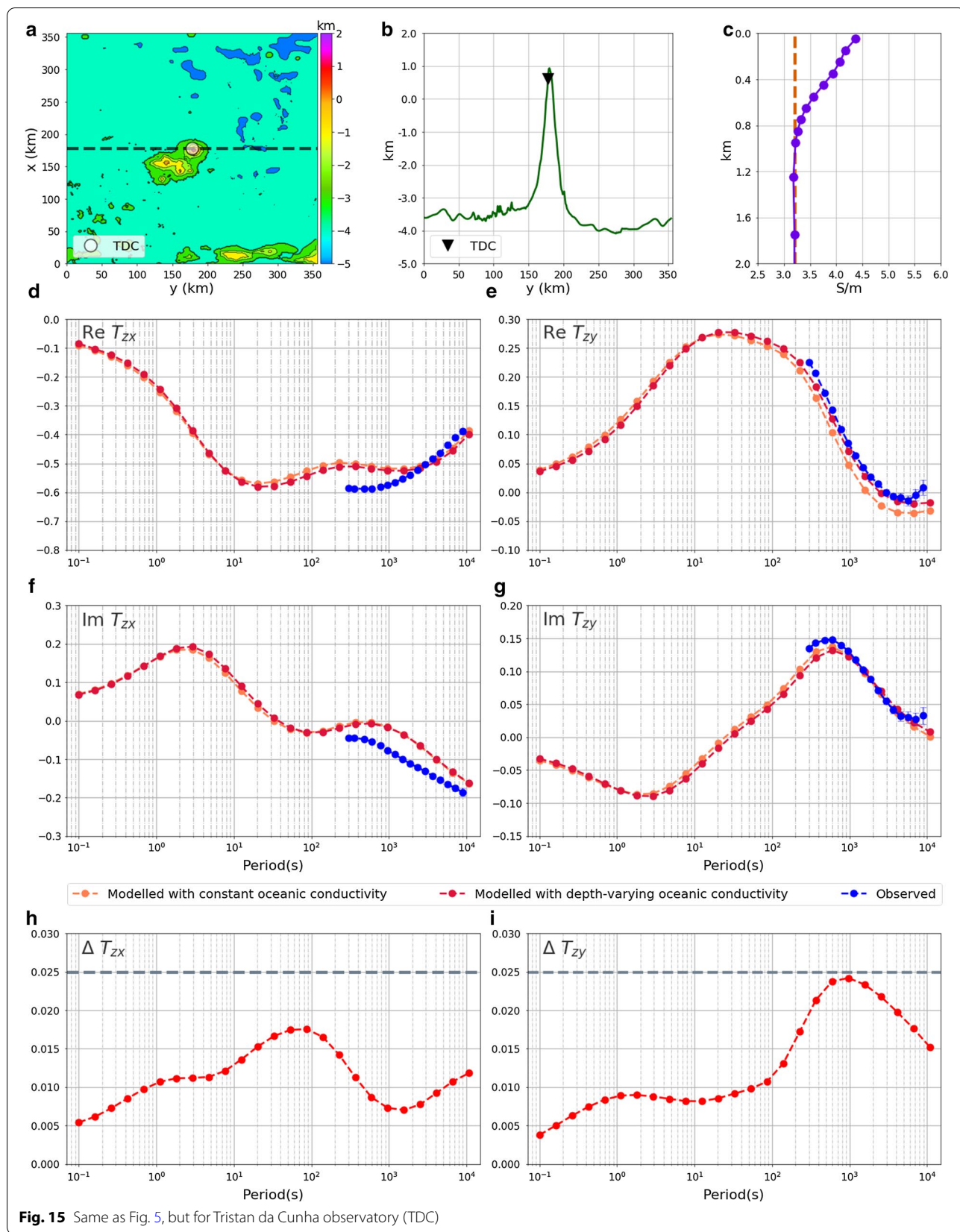


**Fig. 15** Same as Fig. 5, but for Tristan da Cunha observatory (TDC)

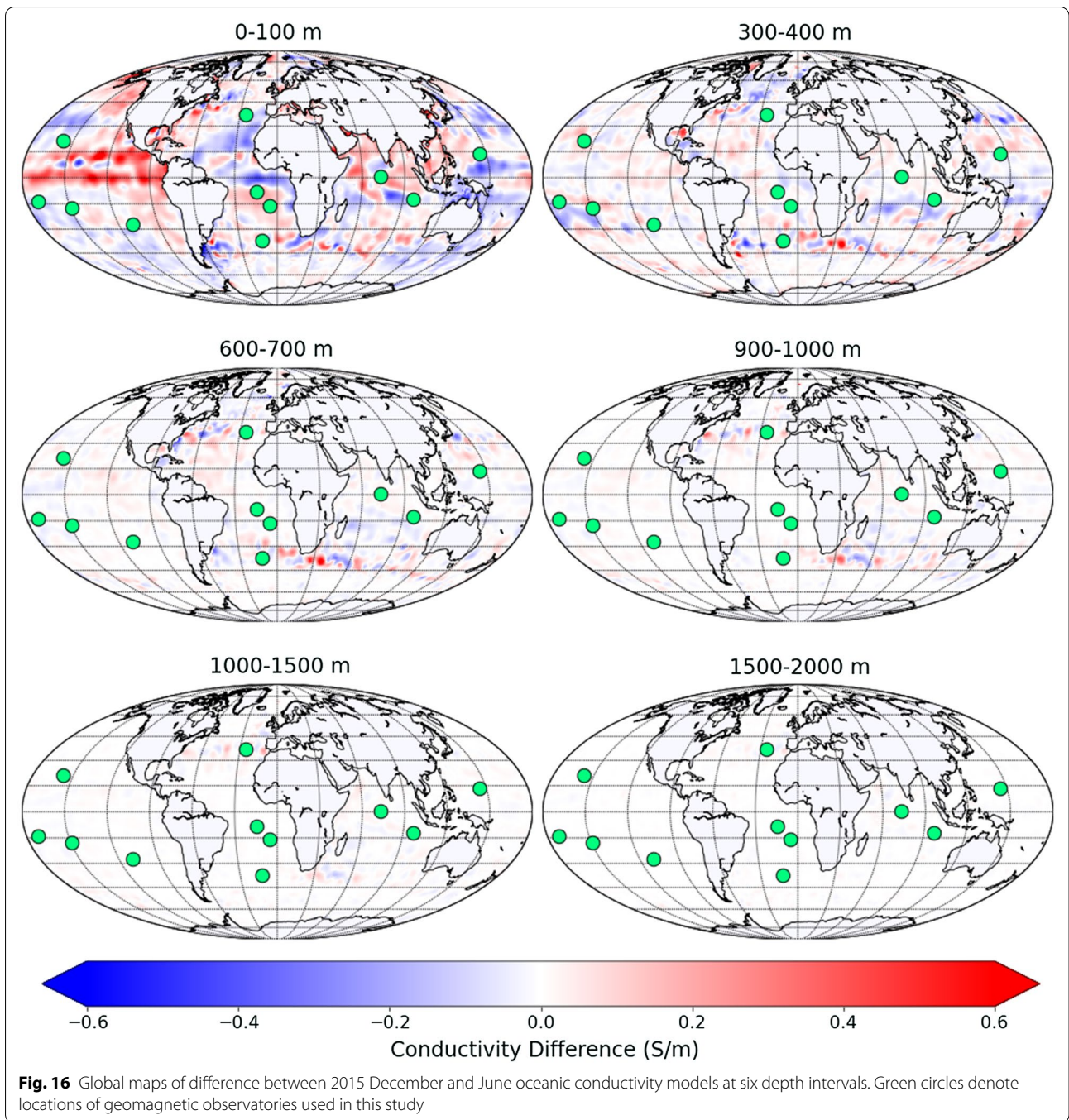


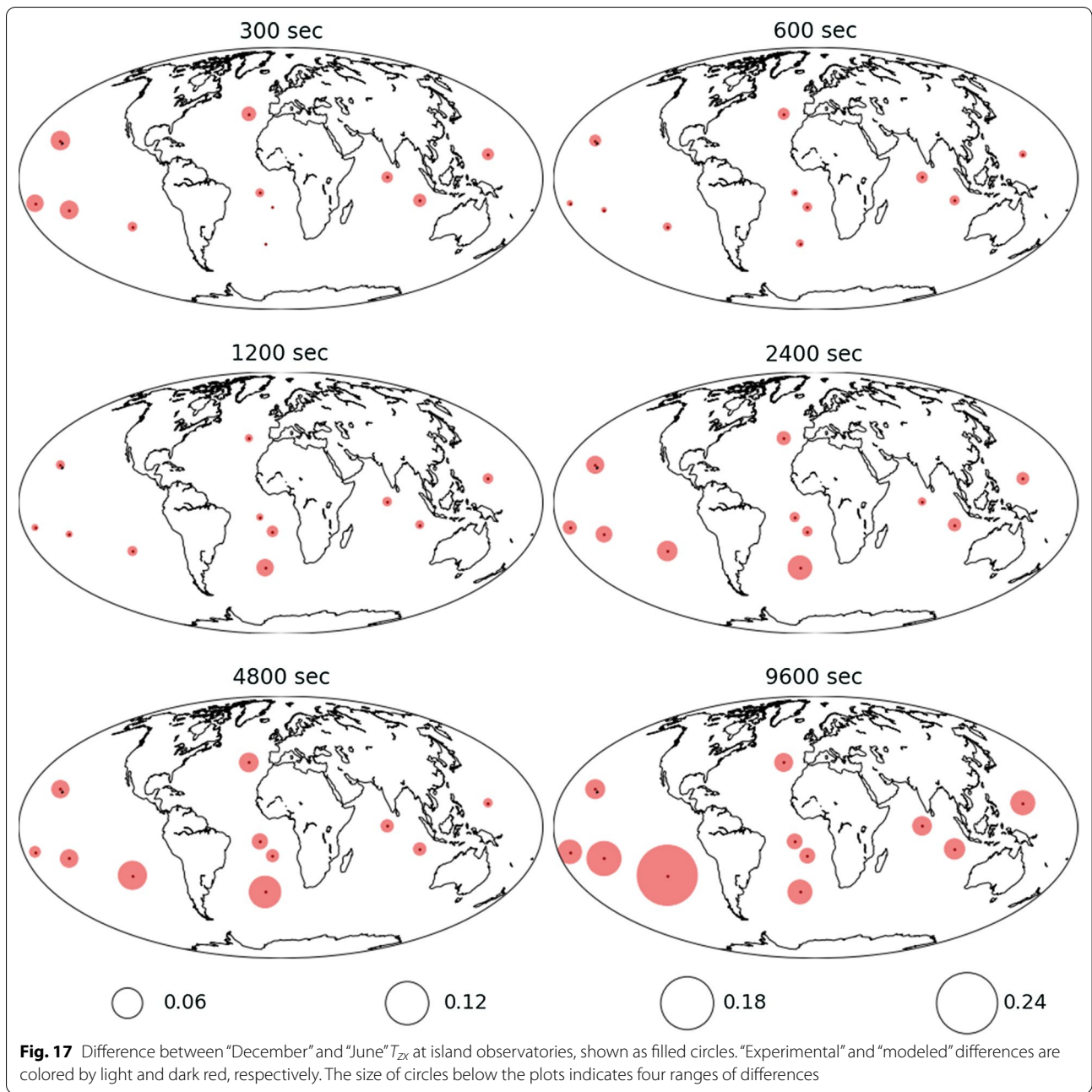
**Fig. 16** Global maps of difference between 2015 December and June oceanic conductivity models at six depth intervals. Green circles denote locations of geomagnetic observatories used in this study

**Effect of time-varying oceanic conductivity**

Figure 16 presents global maps of differences between December and June oceanic conductivity in the same depth intervals as in Fig. 2. As expected, the difference varies laterally, it is the largest at shallower depths (reaching 20 percent of the mean value of oceanic conductivity) and decreases with depth.

Finally, we modeled the effect of time-varying oceanic conductivity on island tippers. The effect is assessed by analyzing the difference:

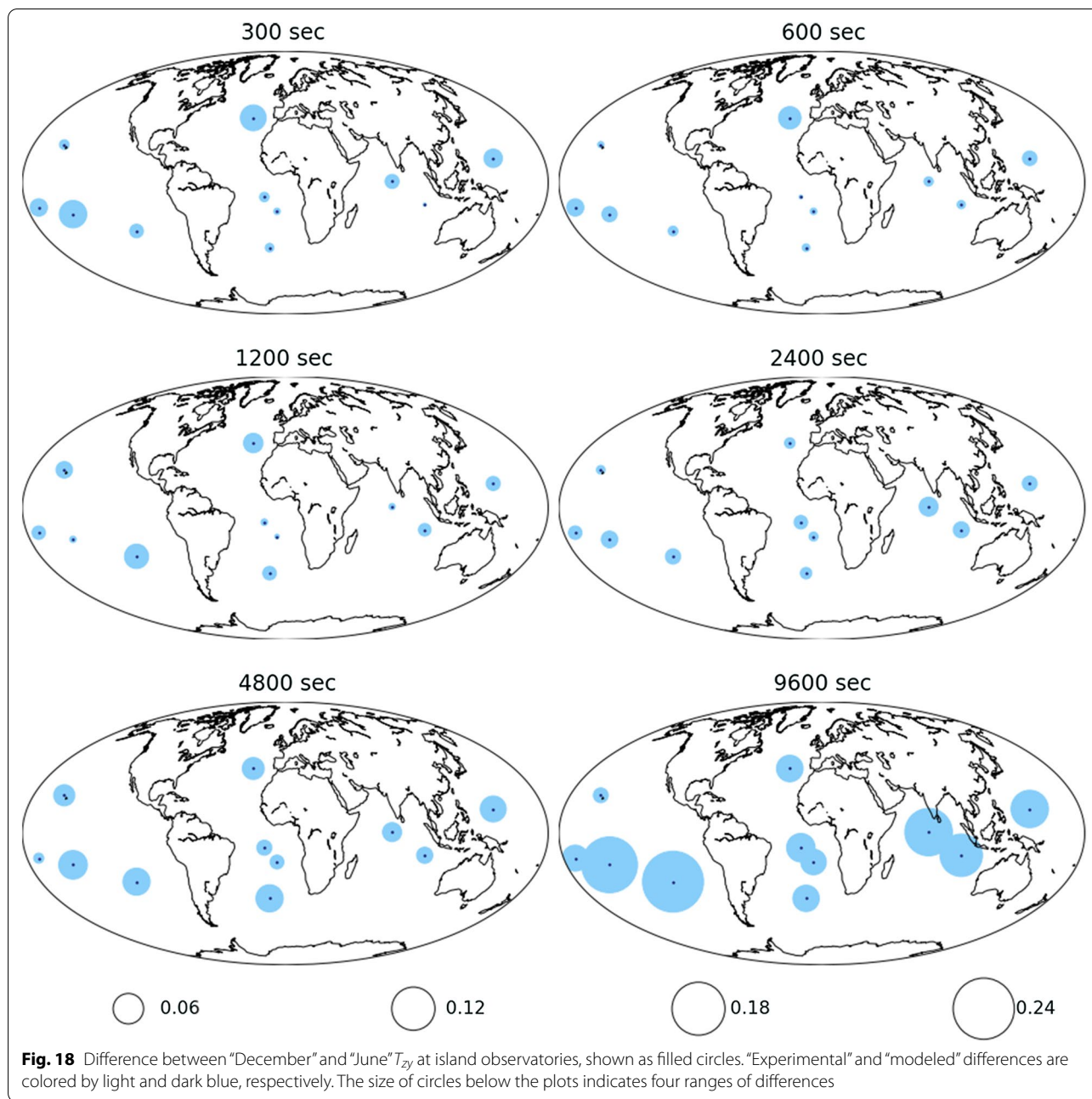
$$\widehat{\Delta T_{zi}} = \sqrt{(\text{Re } T_{zi}^D - \text{Re } T_{zi}^J)^2 + (\text{Im } T_{zi}^D - \text{Im } T_{zi}^J)^2}, \tag{3}$$



where  $i \in [x, y]$ , and superscripts “D” and “J” correspond to December and June results. For the observed (i.e., estimated from the data) tippers, December and June results stand for tippers estimated from observatory data of corresponding 2015 months. As for modeled tippers, these results mean tippers calculated in 3-D models with depth-varying oceanic conductivity models for 2015 December and June months.

In all considered observatories, modeled  $\Delta T_{zx}$  and  $\Delta T_{zy}$  are very small at all periods in the  $10^{-1}$  to  $10^4$  s period

range. Figures 17 and 18 present observed and modeled differences as filled circles on a global map for six representative periods from 300 to 9600 s. Observed and modeled differences are colored in Fig. 17 by light and dark red, and in Fig. 18—by light and dark blue. It is clearly seen that the effect due to time-varying oceanic conductivity is negligible; indeed, the filled circles depicted the modeled difference look as “dots”. It is interesting to note that the temporal variability of the experimental tippers increases with period and, overall, it is larger in  $T_{zy}$ .



### Conclusions

In this study, we performed the first ever analysis of the effects of realistic depth- and time-varying oceanic electrical conductivity on island tippers. The analysis is based on 3-D EM modeling, which was carried out for 11 island observatories located in the Pacific, Atlantic, and Indian Oceans. The conductivity models specific for each observatory were constructed using bathymetry/topography data with the highest spatial resolution available (GEBCO 2019) and a 3-D, time-dependent

and physics-based global model of oceanic conductivity (Petereit et al. 2019). The Cartesian EM forward solver by Kruglyakov and Kuvshinov (2018) was used for tippers' modeling. Modelings were performed in wide period range ( $10^{-1}$  to  $10^4$  seconds) and demonstrated that ocean induction effect in tippers can be traced to periods as short as 0.2 s.

The effect due to depth-varying oceanic conductivity was assessed by comparing the tippers obtained from the depth-varying and depth-constant oceanic conductivity

models. Our model studies show that this effect is tangible in all observatories except for TDC. It exceeds the error floor of 0.025, which is usually assigned to tippers during their 2-D or 3-D inversion, and reaches values of about 0.1 at API, GAN, and HON observatories. The appearance of the effect with respect to period and its strength varies from observatory to observatory. Since depth-varying conductivity profiles are rather similar for all locations, such variability of the effect is most probably due to different bathymetry distributions around the islands.

On the contrary, the modeled effects from time-varying oceanic conductivity appeared to be too small to explain the observed seasonal variations in tippers.

It is worth noting that introducing a more complex ocean conductivity did not lead to an improvement in the agreement between modeled and experimental responses at many observatories. The most possible reason for this is a deviation of local subsurface conductivity structure from the global 1-D section used in the paper. Obviously, to improve the agreement between modeling and experimental tippers, one needs to invert tippers for each location, and thus obtain local conductivity profile beneath each island observatory. Such inversions are out of the scope of this paper, but will be the subject of future study. It is planned to invert island tippers jointly with the longer period responses (cf. Munch et al. 2020) to constrain conductivity throughout the entire depth range. The reliability of the inversions in particular depends on how accurate we represent in the model the oceanic conductivity. In this context, we believe that it is worth effort to use depth-varying oceanic conductivity during inversions provided that these data are considered to be trustworthy.

#### Abbreviations

EM: Electromagnetic; 1-D: One-dimensional; 2-D: Two-dimensional; 3-D: Three-dimensional; OIE: Ocean induction effect; GEBCO: General Bathymetry Chart of the Oceans; MT: Magnetotellurics.

#### Acknowledgements

The authors acknowledge national institutes around the world that operate geomagnetic observatories, and INTERMAGNET ([www.intermagnet.org](http://www.intermagnet.org)) which promotes high standards of observatory practice. We also acknowledge the work of GEBCO group for providing publicly available global bathymetry data. We thank the two anonymous reviewers whose comments greatly improved this manuscript.

#### Authors' contributions

RR estimated tippers from observatory data, prepared 3-D conductivity models, performed 3-D modeling, and analyzed the results. MK provided the 3-D EM modeling code PGIEM2G and assisted RR with the modeling. EM and MK provided the codes for converting global bathymetry/topography and ocean conductivity data into 3-D conductivity models. AK created the concept of the study, and AK and KP supervised the RR's work. JP prepared global oceanic conductivity data. JM obtained and provided SHE and SMA magnetic field data. RR drafted the manuscript. All authors read and approved the final manuscript.

#### Funding

RR was supported by CNPq, Process 133345/2018-1. MK was supported by grant 20-05-00001 from the Russian Foundation for Basic Research. AK was partially supported by the European Space Agency through the Swarm DISC project. KP was supported by FAPERJ (Jovem Cientista do Nosso Estado, Process 202.748/2019). EM was supported by the state assignment of the Schmidt Institute of Physics of the Earth of the Russian Academy of Sciences. JP was supported by the German Research Foundation's priority program 1788 "Dynamic Earth".

#### Availability of data and materials

The results presented in this paper rely on 1 Hz data collected at geomagnetic observatories. These data were digitally filtered to produce 1 min means that are available from the INTERMAGNET data repository.

#### Competing interests

The authors declare that they have no competing interests.

#### Author details

<sup>1</sup> Department of Geophysics, Observatório Nacional, Rio de Janeiro, Brazil. <sup>2</sup> Institute of Geophysics, ETH Zürich, Zurich, Switzerland. <sup>3</sup> Geoelectromagnetic Research Center, Institute of Physics of the Earth, Troitsk, Russia. <sup>4</sup> GFZ German Research Centre for Geosciences, Potsdam, Germany. <sup>5</sup> Institute of Physics of the Earth, Moscow, Russia. <sup>6</sup> Geophysical Center, Moscow, Russia.

Received: 25 October 2020 Accepted: 10 December 2020

Published online: 04 January 2021

#### References

- Araya Vargas J, Ritter O (2016) Source effects in mid-latitude geomagnetic transfer functions. *Geophys J Int* 204(1):606–630
- Aster R, Borchers B, Thurber C (2005) Parameter estimation and inverse problems. Elsevier Academic Press, Waltham
- Banks RJ (1969) Geomagnetic variations and the electrical conductivity of the upper mantle. *Geophys J Int* 17(5):457–487
- Bedrosian PA, Feucht DW (2014) Structure and tectonics of the northwestern United States from EarthScope USArray magnetotelluric data. *Earth Planet Sci Lett* 402:275–289
- Berdichevsky MN, Dmitriev V (2008) Models and methods of magnetotellurics. Springer, Berlin
- Cabanes C, Grouazel A, von Schuckmann K, Hamon M, Turpin V, Coatanoean C (2013) The CORA dataset: Validation and diagnostics of in-situ ocean temperature and salinity measurements. *Ocean Sci* 9(1):1–18
- Chen C, Kruglyakov M, Kuvshinov A (2020) A new method for accurate and efficient modeling of the local ocean induction effects. Application to long-period responses from island geomagnetic observatories. *Geophys Res Lett* 47(8):e2019GL086351. <https://doi.org/10.1029/2019GL086351>
- GEBCO (2019) GEBCO compilation group (2019) GEBCO 2019 grid. <https://doi.org/10.5285/836f016a-33be-6ddc-e053-6c86abc0788e>
- Grayver AV, Kolev T (2015) Large-scale 3D geo-electromagnetic modeling using parallel adaptive high-order finite element method. *Geophysics* 80(6):277–291
- Grayver AV, Munch FD, Kuvshinov AV, Khan A, Sabaka TJ, Toffner-Clausen L (2017) Joint inversion of satellite-detected tidal and magnetospheric signals constrains electrical conductivity and water content of the upper mantle and transition zone. *Geophys Res Lett* 44(12):6074–6081
- Kelbert A, Schultz A, Egbert G (2009) Global electromagnetic induction constraints on transition-zone water content variations. *Nature* 460:1003–1007
- Koyama T, Khan A, Kuvshinov A (2014) Three-dimensional electrical conductivity structure beneath Australia from inversion of geomagnetic observatory data: evidence for lateral variations in transition-zone temperature, water content and melt. *Geophys J Int* 196:1330–1350. <https://doi.org/10.1093/gji/ggt455>
- Kruglyakov M, Kuvshinov A (2018) Using high-order polynomial basis in 3-D EM forward modeling based on volume integral equation method. *Geophys J Int* 213:1387–1401

- Li S, Weng A, Zhang Y, Schultz A, Li Y, Tang Y, Zou Z, Zhou Z (2020) Evidence of Bermuda hot and wet upwelling from novel three-dimensional global mantle electrical conductivity image. *Geochem Geophys Geosyst* <https://doi.org/10.1029/2020GC009016>
- Marcuello A, Queralt P, Ledo J (2005) Applications of dispersion relations to the geomagnetic transfer function. *Phys Earth Planet Inter* 150:85–91
- Morschhauser A, Grayver AV, Kuvshinov AV, Samrock F, Matzka J (2019) Tipplers at island geomagnetic observatories constrain electrical conductivity of oceanic lithosphere and upper mantle. *Earth Planets Space* 71(1):17
- Munch FD, Grayver AV, Kuvshinov A, Khan A (2018) Stochastic inversion of geomagnetic observatory data including rigorous treatment of the ocean induction effects with implications for transition zone water content and thermal structure. *J Geophys Res* 123:31–51
- Munch FD, Grayver AV, Guzavina M, Kuvshinov A, Khan A (2020) Joint inversion of daily and long-period transfer functions reveals lateral variations in mantle water content. *Geophys Res Lett*. <https://doi.org/10.1029/2020GL087222>
- Olsen N (1998) The electrical conductivity of the mantle beneath Europe derived from C-responses from 3 to 720 hr. *Geophys J Int* 133(2):298–308
- Pankratov O, Avdeev D, Kuvshinov A (1995) Electromagnetic field scattering in a heterogeneous earth: a solution to the forward problem. *Izvestiya Phys Solid Earth* 31(3):201–209
- Parkinson W, Jones FW (1979) The geomagnetic coast effect. *Rev Geophys Space Phys* 17(8):1999–2017
- Petereit J, Saynisch-Wagner J, Irrgang C, Thomas M (2019) Analysis of ocean-tide induced magnetic fields derived from oceanic in situ observations: climate trends and the remarkable sensitivity of shelf regions. *J Geophys Res Oceans* 124:8257–8270
- Püthe C, Kuvshinov A (2014) Mapping 3-D mantle electrical conductivity from space: a new 3-D inversion scheme based on analysis of matrix Q-responses. *Geophys J Int* 197(2):768–784
- Rao CK, Jones AG, Moorkamp M, Weckmann U (2014) Implications for the lithospheric geometry of the Iapetus suture beneath Ireland based on electrical resistivity models from deep-probing magnetotellurics. *Geophys J Int* 198:737–759
- Samrock F, Kuvshinov A (2013) Tipper at island observatories: can we use them to probe electrical conductivity of the earth's crust and upper mantle? *Geophys Res Lett* 40:824–828
- Semenov A, Kuvshinov A (2012) Global 3-D imaging of mantle electrical conductivity based on inversion of observatory C-responses—II. Data analysis and results. *Geophys J Int* 191(3):965–992
- Singer B (1995) Method for solution of Maxwell's equations in non-uniform media. *Geophys J Int* 120:590–598
- Straume EO, Gaina C, Medvedev S, Hochmuth K, Gohl K, Whittaker JM, Absul Fattah R, Doornenbal JC, Hopper JR (2019) GlobSed: updated total sediments thickness in the world's oceans. *Geochem Geophys Geosyst* 20: 1756–1772. <https://doi.org/10.1029/2018GC008115>
- Sun J, Kelbert A, Egbert GD (2015) Ionospheric current source modeling and global geomagnetic induction using ground geomagnetic observatory data. *J Geophys Res Solid Earth* 120:6771–6796. <https://doi.org/10.1002/2015JB012063>
- Tietze K, Ritter O (2013) Three-dimensional magnetotelluric inversion in practice—the electrical conductivity structure of the San Andreas fault in central California. *Geophys J Int* 195:130–147
- Tyler RH, Boyer TP, Minami T, Zweng MM, Reagan JR (2017) Electrical conductivity of the global ocean. *Earth Planets Space* 69:156–166
- Utada H, Koyama T, Shimizu H, Chave AD (2003) A semi-global reference model for electrical conductivity in the mid-mantle beneath the North Pacific region. *Geophys Res Lett* 30(4):1194–1198
- Weidelt P (1972) The inverse problem of geomagnetic induction. *J Geophys Res* 77:257–289
- Yang B, Egbert GD, Kelbert ANM (2015) Three-dimensional electrical resistivity of the north-central USA from EarthScope long period magnetotelluric data. *Earth Planet Sci Lett* 422:87–93
- Zhang Y, Weng A, Li S, Yang Y, Tang Y, Liu Y (2020) Electrical conductivity in the mantle transition zone beneath Eastern China derived from L1-Norm C-responses. *Geophys J Int* 221(2):1110–1124. <https://doi.org/10.1093/gji/ggaa059>

## Publisher's Note

Springer Nature remains neutral with regard to jurisdictional claims in published maps and institutional affiliations.

Submit your manuscript to a SpringerOpen® journal and benefit from:

- Convenient online submission
- Rigorous peer review
- Open access: articles freely available online
- High visibility within the field
- Retaining the copyright to your article

---

Submit your next manuscript at ► [springeropen.com](https://www.springeropen.com)

---